

Direct Observation of Magnetoelastic Excitations in a Quasi-1D Spiral Magnet

Chong Wang,^{1,*} Daiwei Yu,^{1,*} Rongyan Chen,¹ Xiaoqiang Liu,¹ Xinyu Du,^{1,†} Lichen Wang,¹ Kazuki Iida,² Kazuya Kamazawa,² Shuichi Wakimoto,³ Ji Feng,^{1,4} Nanlin Wang,^{1,4} and Yuan Li^{1,4,‡}

¹*International Center for Quantum Materials, School of Physics, Peking University, Beijing 100871, China*

²*Comprehensive Research Organization for Science and Society (CROSS), Tokai, Ibaraki 319-1106, Japan*

³*Quantum Beam Science Center, Japan Atomic Energy Agency, Tokai, Ibaraki 319-1195, Japan*

⁴*Collaborative Innovation Center of Quantum Matter, Beijing 100871, China*

We present a systematic study of spin and lattice dynamics in the quasi-one-dimensional spiral magnet CuBr₂, using Raman scattering in conjunction with infrared and neutron spectroscopy as well as first-principles calculation. A rich set of broad Raman bands are observed as spin correlations develop upon cooling. The band energies approximately correspond to sharp optical phonons seen from our Raman and infrared data, and inelastic neutron scattering further reveals that most, if not all, of them are precisely equal to phonon-dispersion energies at the one-dimensional magnetic wave vector. The low-energy bands further exhibit a distinct intensity maximum at the magnetic ordering temperature. Our results point towards the emergence of resonating spin-orbital-lattice textures, or “magnetophonons”, at dispersion intersecting points of phonons and spin excitations.

PACS numbers: 78.30.Hv, 75.50.Ee, 75.85.+t 75.25.-j

How Bosonic excitations in solids may go beyond their standard classifications (*e.g.*, phonons, magnons, etc.) in the presence of strong coupling between different degrees of freedom poses important questions for fundamental research and opportunity for novel applications. Multiferroic spiral magnets [1–4] offer a promising test ground for identifying such effects, since they are expected to exhibit strong coupling between the spin and lattice (concurrent with charge dipolar) degrees of freedom, or “magnetoelastic coupling”. Indeed, mutual control between magnetization and electric polarization via application of electric and magnetic fields, respectively, has been widely demonstrated in these materials [5–9].

In contrast to the extensive experimental characterization and theoretical understanding [10–15] of magnetoelastic coupling effects in the static regime, investigation of their counterparts in the dynamic regime has proved a more demanding task. The challenge is in part brought about by a rich yet diverse set of experimental observations, which include but are not limited to magnetism-induced phonon anomalies [16, 17], spin-lattice mode interactions [18–25], electric-field effect on [26] and optical stimulation of spin excitations [27–31], etc. Some of these effects do not require a spiral magnetic ground state. While they can be regarded as different facets of dynamic magnetoelastic coupling, a unified understanding of the underlying mechanism is still lacking. In particular, while phenomena related to low-energy “electromagnons” [27–30] can be interpreted as electric-field excitation of magnons across a spin-anisotropy gap [31], how phonons and magnons interact and possibly hybridize at higher energies has not been systematically studied. To make progress in this direction, it is desirable to study dynamic magnetoelastic coupling effects in a crystal and magnetic structure that is as simple as possible.

Anhydrous copper (II) bromide CuBr₂ was recently

discovered to be a multiferroic material, with magnetic-order-induced ferroelectricity below the transition temperature $T_N = 73.5$ K [32]. A highly desirable feature of CuBr₂ is its simple crystal structure, which belongs to the monoclinic space group $C12/m1$ (#12) with only three atoms in the primitive cell. The structure consists of edge-sharing CuBr₄ squares that form weakly coupled ribbons running along the b , or C_2 , axis. Each ribbon constitutes a spin-1/2 chain with frustrating nearest- and next-nearest-neighbor spin interactions, which favor a cycloidal spin arrangement along the chain with one-dimensional (1D) propagating wave vector $q_M = 0.235$ in reciprocal lattice units (r.l.u.) [32, 33]. Such a spin pattern breaks inversion symmetry and gives rise to spontaneous ferroelectric polarization, rendering CuBr₂ a system in which strong magnetoelastic coupling can be expected [2–4]. Here, by combining Raman, infrared, and neutron spectroscopic methods and DFT calculations, we report a systematic characterization of pronounced dynamic signatures of magnetoelastic coupling. Our main result is the direct observation of a new type of excitations that most likely originate from dispersion intersecting points of phonons and spin excitations.

Large single crystals of anhydrous CuBr₂ were grown by slow evaporation of aqueous solutions. The high quality of our crystals was confirmed by magnetic susceptibility and specific heat measurements, as well as by single-crystal and powder x-ray diffraction, all showing consistent results as in previous studies [32, 33]. Our Raman scattering measurements were performed in a confocal backscattering geometry using a Horiba Jobin Yvon LabRAM HR Evolution spectrometer, equipped with 600 gr/mm gratings and a liquid-nitrogen-cooled CCD detector. Infrared reflectivity measurements were performed on a Bruker 113 v/s spectrometer with an *in situ* gold over-coating technique [34]. Fresh and optically flat sam-

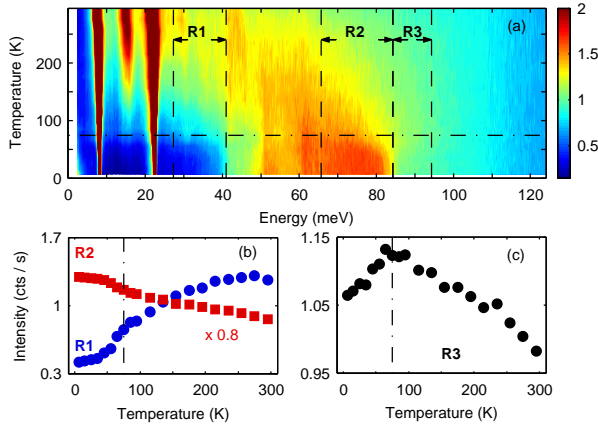


FIG. 1. (a) Variable- T Raman spectra obtained in the *aa* geometry. R1-R3 denote three representative spectral ranges, the intensities averaged over which are displayed in (b) and (c). Dashed-dotted lines indicate T_N .

ple surfaces parallel to the *ab* plane were prepared for Raman and infrared measurements by cleaving crystals right before transfer into vacuum. Our inelastic neutron scattering (INS) experiment was performed on a 14-gram co-aligned sample using the time-of-flight instrument 4SEASONS at J-PARC, Japan, with incident neutron energies of 17 and 55 meV [35–37]. *Ab initio* electronic structure calculations were carried out using the generalized gradient approximation [38] as implemented in the VASP code [39]. To properly describe long-range and local electronic correlations, the DFT-D2 method [40] and the LDA+ U method [41] were employed. The lattice dynamics calculations were carried out using the small-displacement method [42] based on an 8-formula-unit supercell that constitutes a commensurate approximate of the magnetic primitive cell. In the following presentation, the polarization geometries of infrared (Raman) experiments are indicated by one (two) italic letter that specifies the incoming (incoming and scattered) photon polarization along crystallographic directions. Raman scattering intensities are displayed after Bose-factor correction.

Figure 1 displays Raman spectra obtained in the *aa* geometry over a wide temperature and energy range. The color scale is chosen to highlight high-energy features and deeply saturates phonon signals below 30 meV. A clear and broad signal is found to develop as temperature decreases. Its characteristic energy increases with cooling, and intensities averaged over three representative spectral ranges (R1-R3) all show clear anomalies at T_N . The temperature dependence, together with the distribution of spectral weight primarily in the 40-100 meV range at low temperature, which is in accordance with estimated spin interactions [33], indicates that the signal originates from spin excitations presumably dominated by two-magnon scattering [43]. Here we make a few remarks of the data: (1) The signal, although becoming

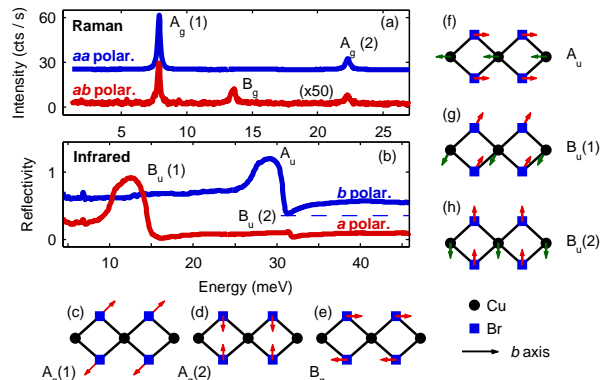


FIG. 2. (a-b) Optical phonons determined by Raman and infrared spectroscopy at 295 K. In (a), two peaks in the *ab*-polarization data are due to polarization leakage from the A_g signals. (c-h) Vibrational patterns of optical phonons at the BZ center. Tilted arrows represent movements perpendicular to the CuBr₂-ribbon plane.

very broad, persists to temperatures well above T_N , suggesting that short-range spin correlations are present even at room temperature. (2) Cooling below T_N depletes intensities below ~ 40 meV, presumably due to formation of partial gaps and/or saddle points in the spin waves. (3) We find a similar signal in the *bb* geometry (not shown), hence the detected excitations belong to the A_g representation of the C_{2h} point group.

There are a total of six optical phonon branches in CuBr₂. At the Brillouin zone (BZ) center, one can infer from symmetry considerations that three modes are Raman-active ($2 \times A_g + B_g$) and the remaining three are infrared-active ($A_u + 2 \times B_u$). Modes belonging to these four representations can be detected in *aa*- (or *bb*-) and *ab*-polarized Raman spectra, and in *b*- and *a*-polarized infrared spectra, respectively. Indeed, we are able to detect all of them, as shown in Fig. 2. Panels (c)-(h) are schematics of the modes, the energies of which determined from our measurements (calculation, $U = 3$ eV), in units of meV, are 7.4 (7.0), 21.8 (21.4), 13.4 (12.5), 27.8 (26.6), 10.1 (8.9), and 31.5 (28.7), respectively. The quoted experimental values are obtained at 295 K and they undergo a slight increase towards 15 K. Given the obviously good agreement between the measurements and the calculation, we can be assured of our exhaustive determination of BZ-center phonons.

We present our main result, Raman spectra obtained in the *bb* geometry, in Fig. 3(a). This geometry is equivalent to *aa* as far as symmetry-related selection rules are concerned, and indeed both of the A_g phonons are clearly observed as sharp peaks. The spectra are nevertheless very different from those in Fig. 2(a) because of difference in the scattering matrix elements. In addition to the two phonons, we observe a rich set of broad bands, which initially gain intensity as temperature decreases,

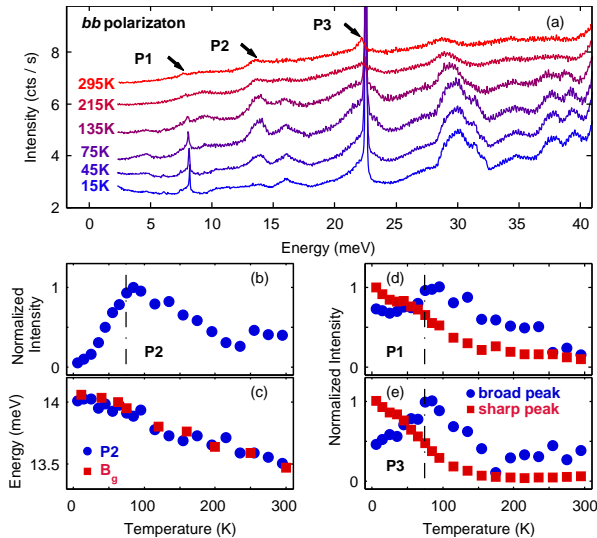


FIG. 3. (a) Raman spectra obtained in the *bb* geometry at selected temperatures, offset for clarity. (b) T dependence of integrated intensity of P2. (c) T -dependent energy of B_g phonon peak measured in the *ab* geometry, in comparison with that of P2. (d and e) T dependence of integrated intensities of broad (circles) and sharp (squares) peaks at P1 and P3. The intensities are determined by fitting the spectra over a nearby energy range to two (broad + sharp) peaks on a linear background. Dashed dotted lines indicate T_N .

and some of which lose intensity upon further cooling below T_N . A nice example is the band at about 14 meV, labeled as P2, which exhibits a distinct spectral weight maximum near T_N and becomes merely visible at 15 K [Fig. 3(b)]. This band is not to be mistaken with, nor can it be due to polarization leakage from, the B_g phonon peak in Fig. 2(a), as the latter is much sharper in energy. Nevertheless, they have nearly the same energy at all temperatures [Fig. 3(c)]. While this can be a sheer coincidence as we will discuss later, it shows that the broad band P2 shares a phonon's generic property of softening with increasing temperature due to anharmonicity.

In addition to P2, we find broad bands that accompany the two A_g phonons at P1 and P3, albeit not exactly at the same energies as the phonons. These bands also exhibit an intensity maximum near T_N [Fig. 3(d-e)], similar to P2. In contrast, the phonon intensities increase monotonically as temperature decreases, which we attribute to temperature-dependent matrix-element effects, since a similar increase is not found in the data obtained in the *aa* geometry. The combined features at P1 and P3 have an asymmetric Fano line shape [44], indicating interference between two scattering processes.

To attain a comprehensive view, a color representation of the full *bb* data set is displayed in Fig. 4(a), along with symbols that indicate energies of optical phonons and the broad bands. Remarkably, each of the six optical phonons is accompanied by a broad band, except

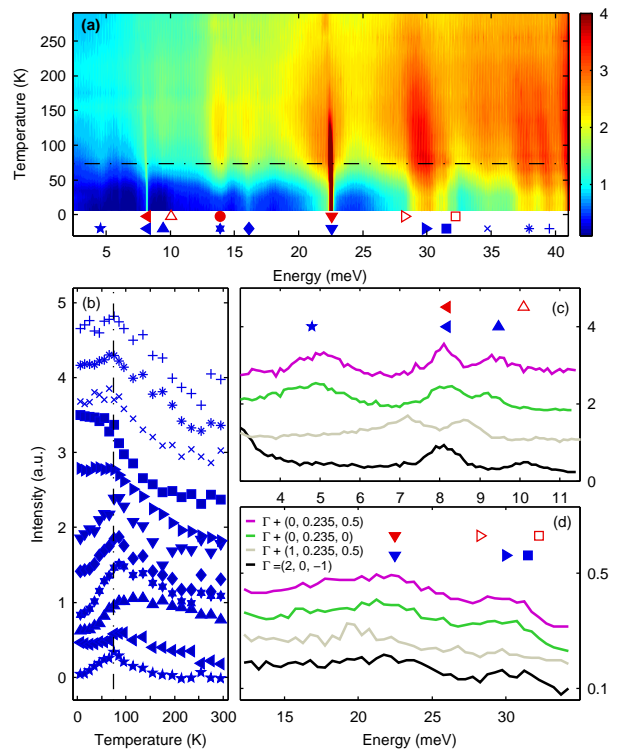


FIG. 4. (a) Color representation of Raman spectra obtained in the *bb* geometry. Dashed dotted line indicates T_N . Symbols at the bottom indicate Raman- (red filled) and infrared-active (red empty) optical phonons and broad Raman bands (blue), and are coded with data and labels in panels (b-d). (b) T dependence of integrated intensities of broad Raman bands, offset for clarity. (c and d) Energy profiles of INS data, measured at 15 K with incident neutron energies 17 (c) and 55 meV (d) at four momentum positions, offset for clarity. The b -polarized A_u phonon (right empty triangle) is expected not to be observable by INS at the measured Γ point.

for the B_g mode at 14 meV which is close to two broad bands. Moreover, all broad bands exhibit an intensity anomaly near T_N [Fig. 4(b)]; the fact that many of them are readily observable at high temperatures is in accordance with the presence of short-range spin correlations above T_N . The results strongly suggest that the broad bands have an origin related to both phonons and magnetism. The bands at energies above 33 meV can be related to double-phonon excitations in a similar fashion and are thus compatible with this assumption.

To further examine the above assumption, it is important to explain the broad bands that *do not* match with optical-phonon energies at the BZ center. To this end, we resort to a comparison with our INS experiment, which allows us to probe phonons away from the BZ center. Our data, obtained at 15 K, are displayed in Fig. 4(c-d), together with characteristic energies labeled after those in Fig. 4(a). At the Γ point, we find an excellent agreement between the optical and INS measurements of the phonons, but there is no INS signal that corresponds to

the broad bands at 4.7 and 9.4 meV [Fig. 4(c)]. Instead, clear INS peaks are found at these energies at momentum (\mathbf{q}) positions that are offset from Γ by q_M along \mathbf{b}^* , or further by 0.5 r.l.u. along \mathbf{c}^* (and anywhere in between). Since phonons disperse only weakly along \mathbf{c}^* which is the direction featured by van der Waals interactions [32], the comparison essentially establishes an empirical connection between the broad bands and phonon dispersions at $q_M \hat{\mathbf{b}}^*$. The INS peak here at about 5 meV arises from the dispersion of an acoustic phonon branch. Since 5 meV is below all optical phonon branches, it is very difficult to find an alternative explanation for the broad band at this energy. In particular, we have checked our momentum-integrated INS data and found no maximum at 5 meV in the generalized phonon density of states.

Another important observation from Fig. 4(c) is that the broad bands do not correspond to INS features observed at the three-dimensional (3D) magnetic wave vector, $\Gamma + (1, 0.235, 0.5)$ [32, 33]. This suggests that the broad bands mainly arise from 1D physics and do not require the 3D magnetic structure, consistent with their temperature dependence. Our INS data above 15 meV were obtained with coarse energy resolution and are insufficient to determine the \mathbf{q} origin of the broad bands above 20 meV [Fig. 4(d)]. The measurement configuration further limited us to relatively small momentum transfers along \mathbf{b}^* , preventing us from detecting the \mathbf{b} -polarized B_g branch [Fig. 2(e)] near 14 meV. Nevertheless, our phonon calculation suggests that the broad band at 14 meV might actually correspond to the dispersion of another acoustic phonon branch at $q_M \hat{\mathbf{b}}^*$, whereas the band at 16 meV might correspond to the dispersion of the B_g optical phonon branch, *i.e.*, the agreement in Fig. 3(c) could be a coincidence.

To explain why Raman scattering can detect excitation energies away from the BZ center, we first note that $\mathbf{q} \neq 0$ phonons can become Raman-active if the lattice translational symmetry is broken, which can fold phonons at $\mathbf{q} \neq 0$ back to the Γ point [45, 46]. However, such a scenario is unlikely to explain our results for the following reasons: (1) The magnetic order in CuBr_2 only breaks translational symmetry in the spin but not the charge density, and is hence not expected to backfold phonons. The associated ionic displacements and ferroelectricity are $\mathbf{q} = 0$ properties. (2) We are not aware of any report of $\mathbf{q} \neq 0$ charge order or structural transition in CuBr_2 . Our neutron diffraction data at low temperatures do not show any satellite Bragg reflections apart from those at the 3D magnetic wave vectors. (3) Even if there were structural satellite Bragg peaks superposed on the magnetic neutron diffraction peaks, they would correspond to $\Gamma + (1, 0.235, 0.5)$ and not $q_M \hat{\mathbf{b}}^*$. (4) A charge order concomitant with a magnetic order is typically found with twice the magnetic wave vector, which is neither seen in our diffraction data nor consistent with $q_M \hat{\mathbf{b}}^*$. (5) In our calculation, we find a stable cycloidal magnetic order in

our supercell, but no associated $\mathbf{q} \neq 0$ lattice distortions can be verified beyond numerical errors. (6) The strong suppression of low-energy bands below T_N [Fig. 4(b)] is very difficult to explain by phonon backfolding, which is expected to be enhanced in the ordered state.

Inferring from Fig. 4(c), we argue that the broad bands may be the signature of a new type of collective excitations that emerge at the dispersion intersecting points of phonons and spin excitations. The new excitations share the phonons' characteristic energies and are “hybrid”, as they involve both lattice and spin degrees of freedom. Hence they can be backfolded to the Γ point by quasi-1D spin correlations and become Raman-active already above T_N . Concerted lattice and spin-flip motions are possible in CuBr_2 due to the strong magnetoelastic coupling, and in the further presence of spin-orbit coupling [33], the emerging excitations can be understood as coherently resonating spin-orbital-lattice textures. Their emergence at the phonon and magnon intersecting points is consistent with the large energy widths of the observed bands due to sampling of phonons at a quasi-1D collection of \mathbf{q} points. Moreover, it naturally explains the intensity decrease below T_N [Fig. 4(b)], since a partial removal of such intersecting points is expected upon the formation of gaps and/or saddle points in the spin-wave spectrum. Finally, we note that the emerging excitations may be related to recent findings in high- T_c cuprate superconductors, with possible consequences in the quasi-static [47, 48] and dynamic [24, 25] regimes.

To summarize, we have observed pronounced signatures of dynamic magnetoelastic coupling in a structurally simple spiral magnet. Our observations can be attributed resonating spin-orbital-lattice textures, or “magnetophonons”, at dispersion intersecting points of phonons and spin excitations. We expect our result to be useful as benchmarks for theoretical developments.

We wish to thank P. Bourges, T. Dong, C. Fang, B. Keimer, D.-H. Lee, J. Park, L.-P. Regnault, F. Wang, and W.-Q. Yu for stimulating discussions. Work at Peking University is supported by NSFC (Nos. 11374024, 11522429, and 11174009) and MOST (Nos. 2013CB921901, 2013CB921903, and 2015CB921302). The neutron experiment at the MLF, J-PARC was performed under a user program (Proposal No. 2014B0032).

* These authors contributed equally to this study.

† Present address: Beijing Institute of Nanoenergy and Nanosystems, Chinese Academy of Sciences, Beijing 100083, China

‡ yuan.li@pku.edu.cn

- [1] N. A. Spaldin and M. Fiebig, *Science* **309**, 391 (2005).
- [2] S.-W. Cheong and M. Mostovoy, *Nature Materials* **6**, 13 (2007).
- [3] D. Khomskii, *Physics* **2**, 20 (2009).

[4] Y. Tokura and S. Seki, *Adv. Mater.* **22**, 1554 (2010).

[5] T. Kimura, T. Goto, H. Shintani, K. Ishizaka, T. Arima, and Y. Tokura, *Nature* **426**, 55 (2003).

[6] N. Hur, S. Park, P. A. Sharma, J. S. Ahn, S. Guha, and S. W. Cheong, *Nature* **429**, 392 (2004).

[7] Y. Yamasaki, S. Miyasaka, Y. Kaneko, J.-P. He, T. Arima, and Y. Tokura, *Phys. Rev. Lett.* **96**, 207204 (2006).

[8] S. Ishiwata, Y. Taguchi, H. Murakawa, Y. Onose, and Y. Tokura, *Science* **319**, 1643 (2008).

[9] Y. S. Chai, S. Kwon, S. H. Chun, I. Kim, B.-G. Jeon, K. H. Kim, and S. Lee, *Nature Communications* **5**, 4208 (2014).

[10] H. Katsura, N. Nagaosa, and A. V. Balatsky, *Phys. Rev. Lett.* **95**, 057205 (2005).

[11] I. A. Sergienko and E. Dagotto, *Phys. Rev. B* **73**, 094434 (2006).

[12] M. Mostovoy, *Phys. Rev. Lett.* **96**, 067601 (2006).

[13] H. J. Xiang, S.-H. Wei, M.-H. Whangbo, and J. L. F. Da Silva, *Phys. Rev. Lett.* **101**, 037209 (2008).

[14] S. Dong, R. Yu, S. Yunoki, J.-M. Liu, and E. Dagotto, *Phys. Rev. B* **78**, 155121 (2008).

[15] X. Z. Lu, X. Wu, and H. J. Xiang, *Phys. Rev. B* **91**, 100405 (2015).

[16] A. F. García-Flores, A. F. L. Moreira, U. F. Kaneko, F. M. Ardito, H. Terashita, M. T. D. Orlando, J. Gopalakrishnan, K. Ramesha, and E. Granado, *Phys. Rev. Lett.* **108**, 177202 (2012).

[17] M. E. Valentine, S. Koohpayeh, M. Mourigal, T. M. McQueen, C. Broholm, N. Drichko, S. E. Dutton, R. J. Cava, T. Birol, H. Das, and C. J. Fennie, *Phys. Rev. B* **91**, 144411 (2015).

[18] P. Dai, H. Y. Hwang, J. Zhang, J. A. Fernandez-Baca, S.-W. Cheong, C. Kloc, Y. Tomioka, and Y. Tokura, *Phys. Rev. B* **61**, 9553 (2000).

[19] F. Moussa, M. Hennion, F. Wang, P. Kober, J. Rodríguez-Carvajal, P. Reutler, L. Pinsard, and A. Revcolevschi, *Phys. Rev. B* **67**, 214430 (2003).

[20] S. Petit, F. Moussa, M. Hennion, S. Pailhès, L. Pinsard-Gaudart, and A. Ivanov, *Phys. Rev. Lett.* **99**, 266604 (2007).

[21] T. Fennell, M. Kenzelmann, B. Roessli, H. Mutka, J. Olivier, M. Ruminy, U. Stuhr, O. Zaharko, L. Bovo, A. Cervellino, M. K. Haas, and R. J. Cava, *Phys. Rev. Lett.* **112**, 017203 (2014).

[22] Q. Zhang, M. Ramazanoglu, S. Chi, Y. Liu, T. A. Lograsso, and D. Vaknin, *Phys. Rev. B* **89**, 224416 (2014).

[23] F. Kadlec, V. Goian, C. Kadlec, M. Kempa, P. c. v. Vaněk, J. Taylor, S. Rols, J. Prokleska, M. Orlita, and S. Kamba, *Phys. Rev. B* **90**, 054307 (2014).

[24] J. J. Wagman, D. Parshall, M. B. Stone, A. T. Savici, Y. Zhao, H. A. Dabkowska, and B. D. Gaulin, *Phys. Rev. B* **91**, 224404 (2015).

[25] J. Wagman, J. P. Carlo, J. Gaudet, G. Van Gastel, D. L. Abernathy, M. B. Stone, G. Granroth, A. I. Kolesnikov, A. T. Savici, Y. J. Kim, H. Zhang, D. Ellis, Y. Zhao, L. Clark, A. Kallin, E. Mazurek, H. Dabkowska, and B. Gaulin, “Neutron scattering studies of spin-phonon hybridization and superconducting spin-gaps in the high temperature superconductor $\text{La}_{2-x}(\text{Sr},\text{Ba})_x\text{CuO}_4$,” (2015), arXiv:1509.08905.

[26] P. Rovillain, R. de Sousa, Y. Gallais, A. Sacuto, M. A. Measson, D. Colson, A. Forget, M. Bibes, A. Barthelemy, and M. Cazayous, *Nat Mater* **9**, 975 (2010).

[27] A. Pimenov, A. A. Mukhin, V. Y. Ivanov, V. D. Trakin, A. M. Balbashov, and A. Loidl, *Nat. Phys.* **2**, 97 (2006).

[28] A. B. Sushkov, R. V. Aguilar, S. Park, S.-W. Cheong, and H. D. Drew, *Phys. Rev. Lett.* **98**, 027202 (2007).

[29] Y. Takahashi, R. Shimano, Y. Kaneko, H. Murakawa, and Y. Tokura, *Nat. Phys.* **8**, 121 (2012).

[30] T. Kubacka, J. A. Johnson, M. C. Hoffmann, C. Vicario, S. de Jong, P. Beaud, S. Grüber, S.-W. Huang, L. Huber, L. Patthey, Y.-D. Chuang, J. J. Turner, G. L. Dakovski, W.-S. Lee, M. P. Miniti, W. Schlotter, R. G. Moore, C. P. Hauri, S. M. Koohpayeh, V. Scagnoli, G. Ingold, S. L. Johnson, and U. Staub, *Science* **343**, 1333 (2014).

[31] D. Senff, P. Link, K. Hradil, A. Hiess, L. P. Regnault, Y. Sidis, N. Aliouane, D. N. Argyriou, and M. Braden, *Phys. Rev. Lett.* **98**, 137206 (2007).

[32] L. Zhao, T.-L. Hung, C.-C. Li, Y.-Y. Chen, M.-K. Wu, R. K. Kremer, M. G. Banks, A. Simon, M.-H. Whangbo, C. Lee, J. S. Kim, I. Kim, and K. H. Kim, *Advanced Materials* **24**, 2469 (2012).

[33] C. Lee, J. Liu, M.-H. Whangbo, H.-J. Koo, R. K. Kremer, and A. Simon, *Phys. Rev. B* **86**, 060407 (2012).

[34] C. C. Homes, M. Reedyk, D. A. Cradles, and T. Timusk, *Appl. Opt.* **32**, 2976 (1993).

[35] M. Nakamura, R. Kajimoto, Y. Inamura, F. Mizuno, M. Fujita, T. Yokoo, and M. Arai, *Journal of the Physical Society of Japan* **78**, 093002 (2009).

[36] R. Kajimoto, M. Nakamura, Y. Inamura, F. Mizuno, K. Nakajima, S. Ohira-Kawamura, T. Yokoo, T. Nakatani, R. Maruyama, K. Soyama, K. Shiba, K. Suzuya, S. Sato, K. Aizawa, M. Arai, S. Wakimoto, M. Ishikado, S. ichi Shamoto, M. Fujita, H. Hiraka, K. Ohoyama, K. Yamada, and C.-H. Lee, *Journal of the Physical Society of Japan* **80**, SB025 (2011).

[37] Y. Inamura, T. Nakatani, J. Suzuki, and T. Otomo, *Journal of the Physical Society of Japan* **82**, SA031 (2013).

[38] J. P. Perdew, K. Burke, and M. Ernzerhof, *Phys. Rev. Lett.* **77**, 3865 (1996).

[39] G. Kresse and J. Furthmüller, *Phys. Rev. B* **54**, 11169 (1996).

[40] S. Grimme, *J. Comp. Chem.* **27**, 1787 (2006).

[41] S. L. Dudarev, G. A. Botton, S. Y. Savrasov, C. J. Humphreys, and A. P. Sutton, *Phys. Rev. B* **57**, 1505 (1998).

[42] A. Togo and I. Tanaka, *Scr. Mater.* **108**, 1 (2015).

[43] P. A. Fleury and R. Loudon, *Phys. Rev.* **166**, 514 (1968).

[44] U. Fano, *Phys. Rev.* **124**, 1866 (1961).

[45] X. Du, R. Yuan, L. Duan, C. Wang, Y. Hu, and Y. Li, *Phys. Rev. B* **90**, 104414 (2014).

[46] M. Bakr, S. M. Souliou, S. Blanco-Canosa, I. Zegkinoglou, H. Gretarsson, J. Strempfer, T. Loew, C. T. Lin, R. Liang, D. A. Bonn, W. N. Hardy, B. Keimer, and M. Le Tacon, *Phys. Rev. B* **88**, 214517 (2013).

[47] S. W. Lovesey, D. D. Khalyavin, and U. Staub, *Journal of Physics: Condensed Matter* **27**, 292201 (2015).

[48] M. Fechner, M. J. A. Fierz, F. Thöle, U. Staub, and N. A. Spaldin, “Quasi-static magnetoelectric multipoles as the order parameter for the pseudo-gap phase in cuprate superconductors,” (2015), arXiv:1510.04844.